A polypropylene fiber phantom to simulate the magnetic susceptibility effects of white matter microstructure at varying orientation to B0

Way Cherng Chen[1], and Karla Miller[1]
[1]Centre for Functional MRI of the Brain (FMRIB), University of Oxford, Oxford, Oxfordshire, United Kingdom

Introduction Structural images generally provide poor discrimination between adjacent white matter pathways. However, contrast between WM fiber bundles has recently been observed using GRE phase imaging (1), T2* mapping (2) and BSSFP (3), all of which are sensitive to magnetic susceptibility. The source of these contrasts has been suggested to relate to magnetic susceptibility shifts associated with different compartments in axonal fibre bundles (1,2,3). To date, however, the actual microscopic field patterns have not been fully characterized. As part of a modelling study that aims to provide this characterization, we constructed a phantom of densely-packed fibres to study the relationship of T2* and GRE phase maps to the orientation to B0.

Methods Phantom construction. The phantom consists of a central cubic region with straightened polypropylene fishing lines (Vantage Pro™ ¼ lbs brown, 13-353-14, 0.35mm) stacked approximately parallel to each other. An outer ring of fishing lines were arranged orthogonal to these fibers in order to approximately match the magnetic susceptibility of the inner square (See Figure 1). This cylindrical shape of the fibre-packed region minimizes the bulk susceptibility effects between different spatial regions when the phantom is rotated. This fishing line phantom is then immersed into a container filled with copper (II) sulphate doped water. Imaging and fitting protocol. The phantom was carefully rotated about the x-axis at the middle of the phantom to obtain 10 different orientations of the inner fiber axis to B0 from 0 to 90 degrees in steps of 10 degrees. T2*, T2 and GRE phase measurements were carried out at each of the 10 orientations. A 2D multi-echo GRE sequence was used to measure the T2* decay. Eight, 2mm-thick interleaved slices were acquired with 6 echoes at TE 20,24,28,32,36 and 40ms (TR = 1500ms, FOV 128 x 128 mm2, matrix 64 x 64, 2 averages and flip 45°). The T2* value was estimated with linear fitting to the logarithm of the magnitude images for even echoes. T2 was measured with a 2D dual-echo spin-echo sequence with 2 echoes at TE 12 and 50ms (TR = 1500ms, FOV 128 x 128 mm2, matrix 64 x 64, 2 averages), and T2 was fitted using the same procedure. GRE phase was obtained from the GRE echoes at TE 4 and 20ms (TR = 1500ms, FOV 128 x 128 mm^2, matrix 64 x 64, 2 averages and flip 10°). The complex conjugate of the raw image of the second echo was multiplied with the raw image of the first echo, the phase image was then extracted and 2D phase unwrapping was performed. The frequency image was calculated by dividing the phase image by the difference in the echo times. The unwrapped phase images were then directly used to obtain the difference in the phase at different orientations (it is assumed that the bulk magnetic field effects across all the orientations are the same due to the geometry of the phantom and a subtraction provides the difference due only to small scale field effects). A 10mm x 10mm middle region at slice 5 was selected for ROI analysis.

Results and discussions The T2* relaxation time decreases when the fibers become more perpendicular to B0 (see Fig.2a). The T2 relaxation time at the different orientations do not show any significant differences (ANOVA test p = 0.1173), indicating that the decrease is due to T2' (since 1/T2* = 1/T2 + 1/T2). This is expected as the dipolar pattern generated by these long structures are at the maximum when perpendicular to B0 thus generating a large distribution of local magnetic field perturbations (4). The T2* measurements show a strong $\sin^2\theta$ dependence (R2=0.994) similar to a study by Yablonskiy et al (4) on a fiber matrix phantom used to mimic the bone structure. Major differences with our phantom include the density of fiber packing and the bulk shape of the phantom. The magnitude of the $\sin^2\theta$ dependence is expected to be dependent on the actual packing of the fibers. The frequency shift (indicated by the phase measurements) shows an increase as the angle to B0 is increased (see Fig.2b), with a similar $\sin^2\theta$ dependence (R2=0.980). In addition to the intrinsic frequency shift due to the microstructure, the frequency shift can also be modulated by susceptibility anisotropy, which might be present due the highly ordered polypropylene molecules. By minimizing the contribution of bulk magnetic susceptibility effects, signal changes can be more definitively attributed to the microstructural properties of the phantom. We observe a similar trend in the fiber phantom to that previously reported in white matter fibre tracts (5,6), supporting the idea that phase and T2* variation in white matter fibers is related to magnetic susceptibility shifts associated with axonal micro-geometry. However, the phase dependence on orientation was unexpected since the dipolar frequency shifts are expected to average to zero in the extra-cylindrical space. Simulations suggest that this may reflect significant partial volume effects for cylinders with diameters that are a sizeable fraction of the voxel dimension, such that the dipolar patterns may not be sufficiently contained within the voxel to average to zero. Thus, slight shifts in the voxel FOV may alter the frequency content enough to introduce an apparent phase dependence that would be averaged out over a larger FOV. This may represent an important design criterion for future phantom construction.

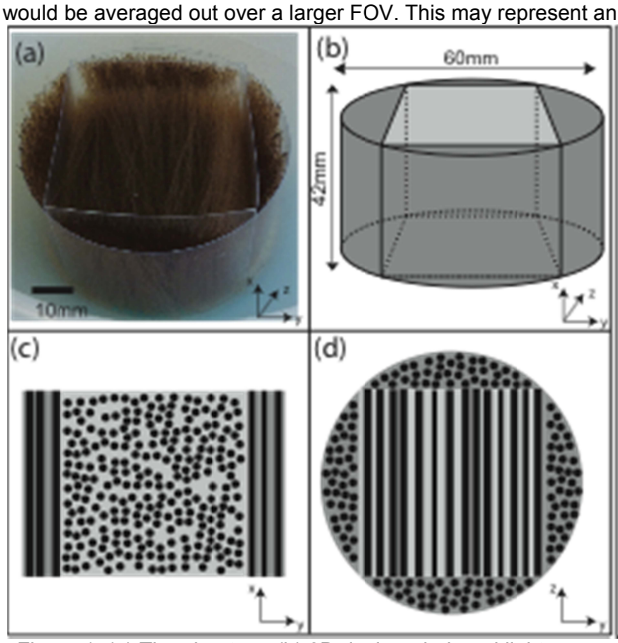

Figure 1. (a) The phantom. (b) 3D design: dark and light gray regions contain vertical and horizontal fibers, respectively. 2D cross sections along vertical (c) and horizontal (d) axes.

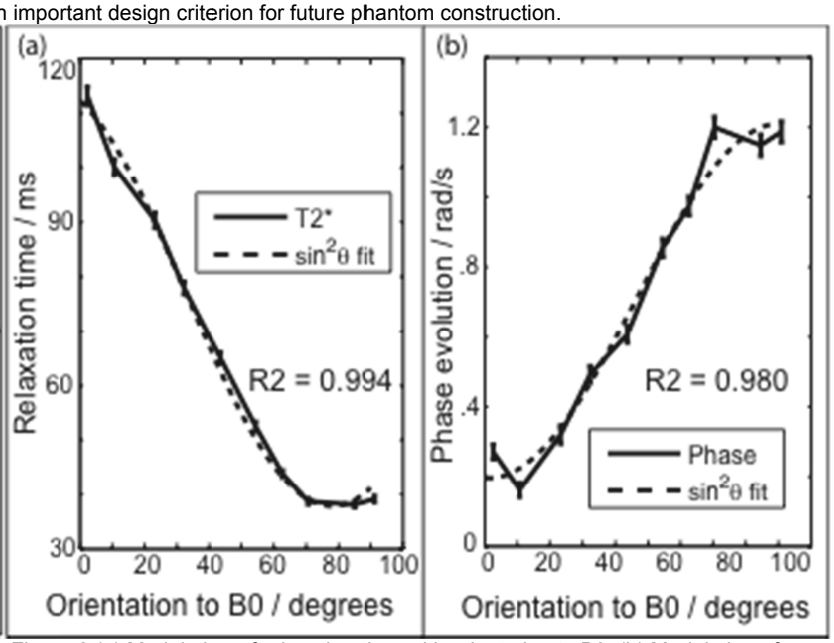

Figure 2 (a) Modulation of relaxation time with orientation to B0. (b) Modulation of phase evolution with orientation to B0.

References (1) Duyn et al PNAS 2007. (2) Li et al NeuroImage 2006. (3) Miller et al MRM 2010. (4) Yablonskiy et al MRM 1997. (5) Bender et al NMR biomed 2010. (6) Denk et al NMR biomed 2010.